Numerical Methods in Civil Engineering

Air Pollution Variation During COVID-19 Pandemic Using Satellite and On-site Measurement Data in Six Provinces in Iran

Maryam Zare Shahne[*], Amirhossein Noori[**], Mehdi Alizadeh Attar[***]

ARTICLE INFO

RESEARCH PAPER

Article history:
Received:
July 2024
Revised:
September 2024
Accepted:
December 2024

Keywords:
COVID-19, Air pollution, on-site concentration, satellite data, Iran

Abstract:

In the present study, the temporal variation of Sentinel-5P TROPOMI-derived air pollutants (NO_2 and SO_2,) and MODIS-derived AOD were examined by using satellite missions in six air pollution hotspot provinces, including Isfahan, Tabriz, Mashhad, Tehran, Ahvaz, and Guilan in Iran for contemporaneous time periods before (as a baseline period), and during the epidemic, including the first wave lockdown period of the COVID-19 outbreak, from the 22nd of February, 2019, to the 22nd of February, 2021. The results revealed that the mean ratio of NO_2 and SO_2 has not varied drastically in the considered provinces. These column concentration ratios for all months were within the range of +2%(Tehran) to -6% (Tabriz). In comparison, the ratio of variance is more considerable, especially for Guilan province, a tourist attraction province, even in terms of travel restrictions and lockdowns in Iran. The AOD distribution map and its trend illustrated that Guilan, Khorasan-Razavi, and Tabriz had become more pollutants after the outbreak due to changes in tourist patterns and emission inventories. Based on wavelet transform, implemented on ground-measurements of $PM_{2.5}$, the aerosol concentration increased in early 2021 from the value in the baseline period, due to eased restriction and expansion of public COVID-19 vaccine in all considered provinces.

1. Introduction

In the past decade, rapid industrialization and urbanization have led to the enormous consumption of fossil fuels [1]. As a result, the atmospheric pollutants grew substantially throughout the globe, deteriorating the air quality. Moreover, One of the consequences of air pollution is its harmful and destructive effects on human health, reducing life expectancy, reducing workplace productivity, and environmental impacts, such as reducing visibility and affecting climate and ecosystems [2-4].

Air pollutants, including nitrogen dioxide (NO2), sulfur dioxide (SO2), and particulate matter (PMs), have destructive health effects, depending on the chemical and physical structures, including cardiovascular, respiratory disease, asthma, lung cancer, ventricular hypertrophy, Alzheimer's, and Parkinson's diseases [5-9]. This issue leads to increased treatment costs and work pressure on physicians and, in the long run, will cause mental problems such as fatigue and burnout of treatment staff [10, 11].

The remote sensing method uses satellite data and images to monitor various quantities, including pollution monitoring [12, 13]. Compared to traditional on-site measurement, satellite-based remote-sensing technology facilitates a deeper understanding of the long-term spatiotemporal patterns of air quality on a different scale. The Google Earth Engine (GEE) platform has integrated different satellite imagery resources and geospatial datasets including Landsat, Sentinel, and MODIS. Satellite data can predict and warn of air quality in the medium and long term due to their availability, high spatial resolution, and coverage of a wide range of study areas. Hence, satellite data played a critical role in understanding air quality during the COVID-19 pandemic by providing real-time, large-scale observations of atmospheric pollutants. As global lockdowns significantly reduced human activity, especially industrial and transportation emissions, satellites allowed scientists to observe unprecedented changes in air pollution levels

[*] *Corresponding author: Assistant Professor, Department of Civil and Environmental Engineering, K.N. Toosi University of Technology, Tehran, Iran, maryam_zare@kntu.ac.ir, +989122098876*
[**] *Boston university, Email: amirhosseinnoori1996@gmail.com*
[***] *Department of Civil and Environmental Engineering, Sharif University of Technology, Tehran, Iran.,*

https://doi.org/10.61186/NMCE.2407.1067

including tracking pollutant reductions, global and regional comparisons, and long-term trend analysis [14, 15].

Coronavirus disease, an infectious illness caused by the SARS-CoV-2 virus, has been around since late 2019; in Wuhan, China, it spread and, after a while, spread worldwide [16, 17]. This disease pandemic has affected more than 513 million people worldwide [18]. Studies have been conducted to investigate the association between exposure to poor air quality and increasing rates of morbidity and mortality due to COVID-19. Some scientists have proposed that elevated levels of air pollution may worsen the effects of COVID-19 by compromising respiratory health and increasing vulnerability to severe outcomes [19-21].

By mid-2020, the first empirical studies started to emerge. These studies were primarily correlational, using data from COVID-19 cases and air quality indexes to investigate possible relationships. These studies found that areas with higher levels of pollutants such as $PM_{2.5}$, NO_2, and ozone had higher COVID-19 mortality rates. The correlation between long-term exposure to air pollution and increased vulnerability to severe COVID-19 outcomes was a key finding. Also, air quality exhibited unpredictable and varied behavior during the COVID-19 pandemic, revealing a complex relationship between COVID-19 mortality and pollutant exposure, including NOx, SOx, and particulate matter (PMs). These findings highlight the intricate interactions between environmental factors and health outcomes during the pandemic [19].

Moreover, there are few studies investigating of the effect of coronavirus lockdown on air pollution based on remote-sensing measurements in the world [21-23]. Most of the results indicated that the NO_2 levels were the most significant contributors to mortality caused by the COVID-19 [23, 24]. Moreover, in some significant studies conducted in Iran and other regions, Satellite-based concentrations varied more significantly in the first year of lockdowns than in the second year of pandemic. [25, 26].

Meta-analyses and multi-country studies confirm previous findings while providing a more refined understanding of the roles of specific pollutants. The previous studies indicated the decline of NO_2 and CO concentrations during the lockdowns (Norouzi and Asadi 2022). Moreover, NO_2 had the most significant effect on the density of confirmed cases among all pollutants in the second year of pandemic [27].

Some studies in 2024 explored the use of satellite data to predict COVID-19 hotspots based on air quality, providing a new tool for public health officials to manage future outbreaks. By 2024, research on air quality and COVID-19 has become more sophisticated, leveraging advanced technologies and addressing broader issues such as COVID, climate change, and social equity. These studies continue to inform public health strategies, ensuring that lessons learned from the COVID-19 pandemic are applied to future global health challenges. These studies found that individuals with prolonged exposure to high levels of air pollution were more likely to experience persistent respiratory and cardiovascular issues post-COVID-19 [28, 29].

In general, the intensity and extent of restrictions caused by the coronavirus vary over different periods of time. The lack of monitoring of the changes in air pollutant concentrations in Iran, during two continuous and contemporaneous time periods before (as a baseline period and pre-lockdown year) and during the epidemic has motivated the authors to consider a broader scale of the mentioned pollutants as the index for monitoring the pollutants' trend shifts. To be more precise, this paper simultaneously investigates spatial and temporal pollutant distribution shifts before and during the COVID-19 pandemic.

The focus of this study is to determine the variation of NOx, SOx, and aerosol optical depth (AOD) based on remote sensing data in the two periods, before and during the pandemic in six megacities in Iran. To do this, the median of these parameters was extracted at the considered cities for two years from the 22nd of February, 2019 to the 22nd of February, 2020 (before the COVID-19 outbreak) and the 22nd of February, 2020 to the 22nd of February, 2021 (during COVID pandemic and before wide and public COVID-19 vaccine) by means of freely available Sentinel-5P and MODIS satellite datasets. The Google Earth Engine (GEE) platform is used for the retrieval and processing of satellite imagery, and data analyses. The insights on air pollution during COVID-19 in Iran presented in this study can be invaluable for policymakers in understanding the public health impacts of COVID-19, guiding decisions to control its spread, and planning effective strategies for managing similar situations in the future.

2. Material and Methods

2.1 Study Areas

The authors have chosen six main provinces in Iran to investigate the seasonal variation of the trends of NO2 and SO2 before the COVID-19 pandemic and after the pandemic. These six provinces are Tehran, Khuzestan, Isfahan, Khorasan-Razavi, Tabriz, and Guilan, containing the most megacities in Iran. Demographic information on the selected area is presented as supplementary materials (A1). The locations of the study areas are shown in Fig 1. These provinces have relatively critical air pollution conditions and frequently face critically high pollutant levels due to various pollutant sources, including mobile sources, industrial activities, and biomass burning [30-32].

In this study, air quality data (i.e., NO2 and SO2 and AOD) has been extracted from Sentinel-5P and MODIS Satellite

during two study periods from the 22nd of February 2019 to the 22nd of February 2020 (before the COVID-19 outbreak) and the 22nd of February, 2020 to the 22nd of February, 2021 (during COVID pandemic and before wide and public COVID-19 vaccine).

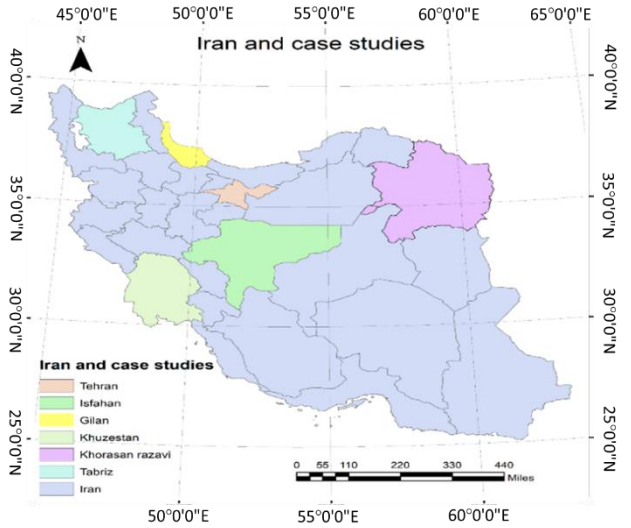

(a)

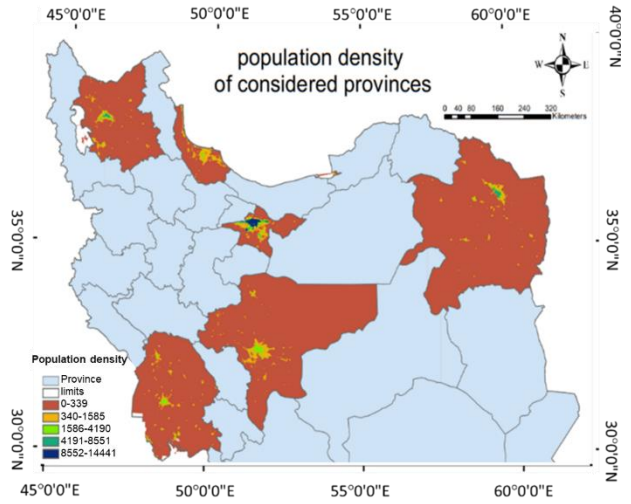

(b)

Fig. 1: a) The location of study areas, b) Population density of considered provinces

2.2. Data collection

Long-term studies of pollutants are essential in providing accurate information for managers to develop air pollution crisis management strategies [33-35]. Two sets of the newest satellites that can monitor air pollution are the Moderate resolution Imaging Spectroradiometer (MODIS) sensor, flown on NASA's Earth Observing System (EOS) satellite, and the Sentinel-5 satellite from the Copernicus project series of satellites of the European Space Agency [36, 37].
Sentinel-5P has a daily temporal resolution, enabling it to monitor global air quality daily [15]. Sentinel-5P carries the TROPOMI sensor, which can measure vast radiation spectral bands, including ultraviolet-visible, near-infrared, and short-wave infrared. Hence, air pollutants such as NO2, O3, CH2O, SO2, CH4, and CO spatial concentrations could be accurately obtained using Sentinel-5P. Sentinel-5P provides data at two processing levels, which are L1B and L2. Since the L2 product of this satellite provides multiple-layer products, including products for diverse pollutants such as SO2, NO2, and O3, it suits the objective of this study [15, 37]. Using satellite data for air quality monitoring presents several potential limitations, including issues with spatial and temporal resolution, as well as interference from cloud cover and weather conditions.
In order to pursue the paper's objective, monthly offline L2-NO2 products and L2-SO2 were used for the periods' before the pandemic, as a baseline period (between the 22nd of February 2018 to the 22nd of February 2019) and after the pandemic (between the 22nd of February 2020 to the 22nd of February 2021), ensuring daily coverage of NO_2 and SO_2 for these two periods. Moreover, in order to compare the pollutant fluctuation before and during the pandemic, the Google Earth Engine tool was used to calculate the median of NO_2 and SO_2 for the year before the pandemic and the year after the pandemic. In other words, for each period (i.e., before and during the pandemic), a single pollutant spatial distribution map has been produced, showing the median pollutant of these periods.
The MODIS satellite has an acceptable spatial resolution. This sensor was mounted on NASA EOS 1's first satellite, the Terra, and launched on the 18th of December, 1999. The sensor is also mounted on the Aqua satellite, which was put into orbit on the 03rd of May, 2002 [36, 38]. The MODIS sensor has 36 bands, 11 of which are in the visible light range, nine bands in the near-infrared range, six bands in the thermal infrared, four bands are set in the short-wave infrared range (SWIR2), and six bands are set in the long-wave infrared range (LWIR3) [39]. The resolution of this sensor's bands varies between 250 meters to 1000 meters. This paper used MODIS to gather information about the distribution of AOD pollutants in all provinces. This parameter described the extinction of light by aerosol particles when passing through the atmosphere, and it was a good representative parameter for the probability presence of fine aerosol emitted in mobile sources [38]. Utilizing free and accessible satellite data offers a highly efficient alternative to the limited availability of ground-based measurements in Iran. In this study, all data were analyzed and extracted using Google Earth Engine, an open-source geospatial analysis platform with planetary-scale capabilities. This powerful tool allows for extensive data processing and analysis through its JavaScript-based programming environment, significantly enhancing research potential.

2.3. Data processing

2.3.1. Statistical analysis

This study used data analysis methods to probe the shift in the NO2 and SO2 pollutants trends (based on satellite data) before and during the pandemic. To be more precise, the mean and variance of the median spatial distribution of pollutants before and after the pandemic were calculated to compare the pollutant distribution shifts. The variance of air pollutant concentration is a crucial statistical measure for understanding the distribution of pollutants due to measuring dispersion and variability, identifying pollution hotspots, and assessing temporal and spatial trends. In other words, variance is essential for understanding the distribution of air pollutants because it provides insights into the consistency, extremes, and patterns of pollution. This understanding helps in assessing risks, identifying critical areas, improving models, and designing effective air quality management strategies. In the following, a brief description of variance will be given. A variance is a statistical tool that discloses information about the distribution of data. By definition, variance is the average squared difference from the mean value of the data [40]:

$$S^2 = \frac{1}{n-1}\sum(O_i - \bar{O})^2 \quad (1)$$

Where S^2 is the sample variance, n number of observations, O_i the value of one observation and $\bar{O}$ Mean of the observations.

In order to compare the monthly variation of pollutants before and after the pandemic root mean square method was utilized. Regarding the RMSE concept, RMSE calculates the mean square of the values of two graphs [41]:

$$RMSE = \sqrt{\frac{1}{n}\sum_{1}^{n}\left(S_{during} - S_{after}\right)^2} \quad (2)$$

2.3.2. Mathematical model: Wavelet transformation

Wavelet transformation is a powerful mathematical tool that allows the decomposition of time-series data into various frequency components, making it particularly useful for analyzing non-stationary signals like air pollutant trends. In air quality studies, pollutant concentrations often exhibit both short-term fluctuations (daily or seasonal variations) and long-term trends (yearly or decadal shifts). Wavelet transformations help in disentangling these patterns by capturing localized variations in time, unlike traditional Fourier analysis, which only focuses on frequency.

In general, the concentration of air pollutants is influenced by a variety of factors, resulting in concentration time series with noisy features. As a result, these noisy features may limit our ability to accurately establish the association between past and future behaviors. As a kind of data preparation, the wavelet transform integrates signals in the frequency domain to produce the original signal, which allows us to obtain information defining the signal's behaviors and extracting its frequency components [42]. By leveraging the discrete wavelet transform (DWT) to decompose the original data, we can more precisely analyze and mitigate the impact of noisy features on air pollution prediction. This advanced approach enhances the accuracy of predictions by isolating and addressing the influence of noise, leading to more reliable and actionable insights into air quality. The mathematic foundations of wavelet transform are outlined below [43]. If it is possible to integrate the square of x(t), the mathematical basis of the continuous wavelet transform (CWT) of x is described as:

$$W_{a,b}(t) = \int_{-\infty}^{+\infty} x(t)\frac{1}{\sqrt{|a|}}\phi\left(\frac{t-b}{a}\right)dt, a \neq 0, b \in R \quad (3)$$

Where x(t) is the original signal, φ(t) is the wavelet function and b and a are the time-centered parameter and scale parameter respectively. x(t) is defined as shown as follows:

$$W_x(a,b) = < x(t), W_{a,b}(t) > = \frac{1}{\sqrt{|a|}}\int x(t)\overline{\phi\left(\frac{t-b}{a}\right)}dt \quad (4)$$

The wavelet can be compressed or stretched by adjusting the value of a, while the wavelet function can be shifted to the left or right by adjusting the value of b.

However, data decomposition is complicated by CWT since the signal is not split up into frequency components. Thus, the discrete wavelet transform (DWT) is frequently used to deconstruct the data in order to avoid the information redundancy created by the continuous wavelet transform, in which the signal is separated into its frequency components depending on amplitude, i.e. breaking the original signal down into its approximate signal namely A and its detail components D. More precisely, the low-frequency signal, denoted by A and represents the main elements of the original sequence. While the high-frequency signal, denoted by D and provides additional details. The decomposition process is iteratively applied to the prior decomposed signal components until the required decomposition level is achieved [44]. Hence, when wavelet transformation is applied to air pollutant trends, it can highlight seasonal patterns, anomalies, and long-term trends. In the context of air quality during the COVID-19 pandemic, wavelet transformation can be used to observe the immediate drop in pollutants due to lockdowns, while also identifying how pollution levels rebounded over time. This method provides insight into how short-term changes (like reduced traffic) interact with broader pollution patterns.

In this paper, the original signal is decomposed into one low-frequency signal and two high-frequency signals. The original sequence is decomposed as follows:

$$X = A_2 + D_1 + D_2 \quad (5)$$

As the exact value of fine particulate matter cannot be accessible through Sentinel-5P and MODIS satellite, the DWT was applied in field measurement of fine particulate matter, in order to examine the pollutant behaviors in this pandemic. In this study, we have studied the daily $PM_{2.5}$ concentration in five provinces, excluding Guilan provinces, because of the lack of data in only one of its stations. By applying wavelet transformation to the analysis of PM trends, we can effectively decompose these time series data into different frequency components, allowing us to capture both short-term fluctuations and long-term patterns. This method enhances our ability to identify and interpret periodic behaviors, seasonal variations, and abrupt changes in pollutant levels, providing a more detailed understanding of the underlying dynamics and potential influencing factors.

3. Results and discussion

3.1. Satellite components variation

This paper, calculated the monthly mean and variance of NO2 and SO2 levels in all six provinces based on remote-sensing techniques during two contemporaneous time periods before and after the epidemic lockdown. Figure 2 compares the ratios of means and variances of NO2 and SO2 for two considered periods. This figure illustrates that the mean of NO2 pollutants has not altered magnificently. The mean monthly NO2 concentration in all provinces increased during the lockdown in 2020 compared to the same period in 2019. The ratios of mean levels of NO2 in two continuous time periods ranged from 1.05 to 1.15, except Khuzestan (0.95). Also, the mean variances of NO2 concentration increased during the pandemic, except in Khuzestan and Tehran. So, the NO_2 concentrations showed a relatively high temporal variation across the COVID-19 outbreak. It can be interpreted that the lockdowns and quarantines could not decrease the NO_2 levels in these provinces in Iran. The range of the ratio of the mean value of NO2 is between +2% (Tehran) and -6% (Tabriz). Whereas, in the case of NO2 variance, the fluctuation between the pandemic duration and before the pandemic is significant. These results are a bit different from other studies, which they reflected a decrease in NO_2 levels in the COVID-19 outbreak in Turkey and China [20-22].

The maps of pollutant levels for these provinces before and during the pandemic are described in Figure 3. The results convey that the median of pollutant concentrations did not change significantly before and during the pandemic. However, in Guilan province, NO_2 and SO_2 have shown some increase in pollutant concentration after the pandemic due to the increase in traveling to Guilan. Moreover, in the case of other cities' lack of industrial activity data, a conclusive result was not available. The results also show good consistency of ground-based measurement at air pollutants monitoring sites by the remote-sensing measurements in these locations [45].

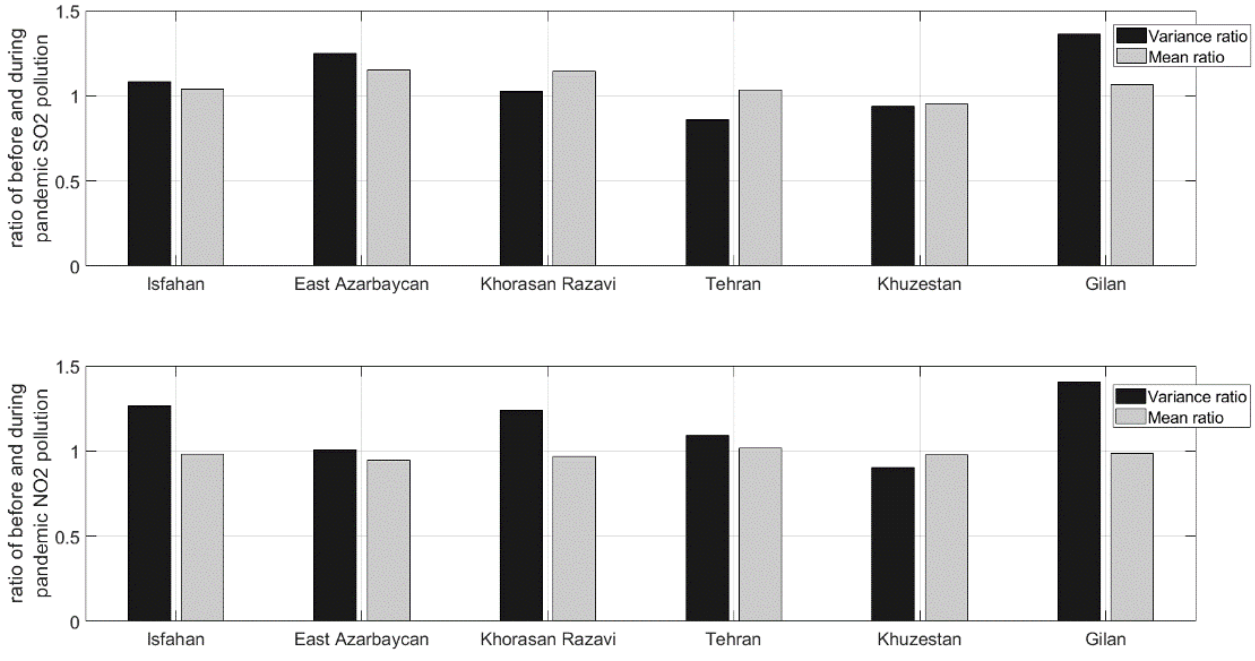

Fig.2: Mean and Variance Ratio of NO_x and SO_x during and before the pandemic

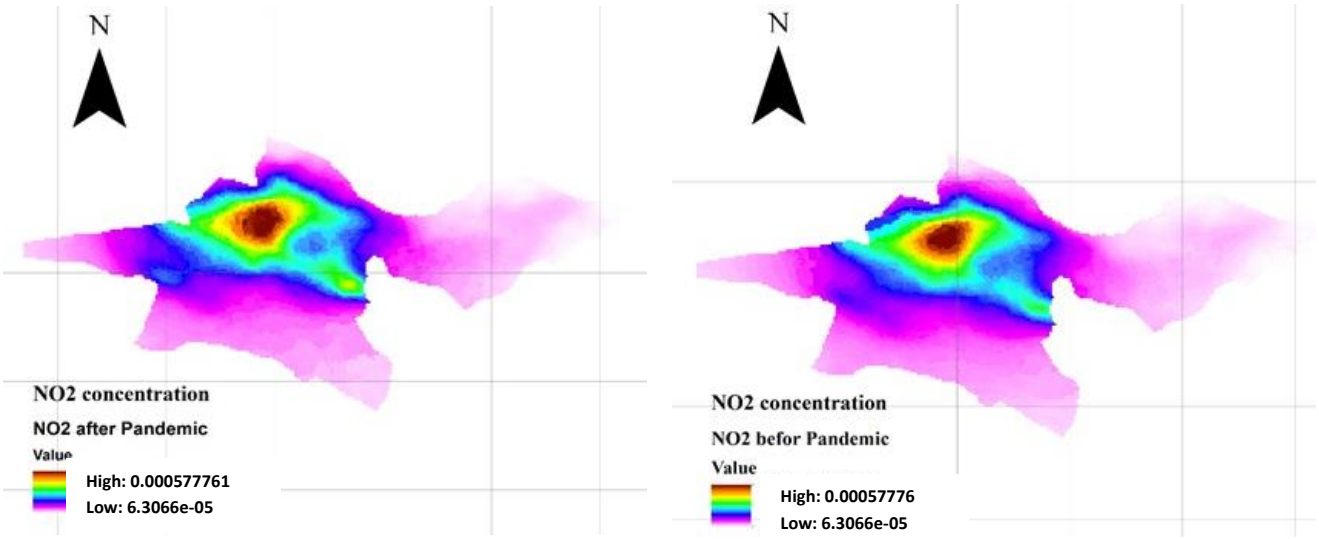

(a)

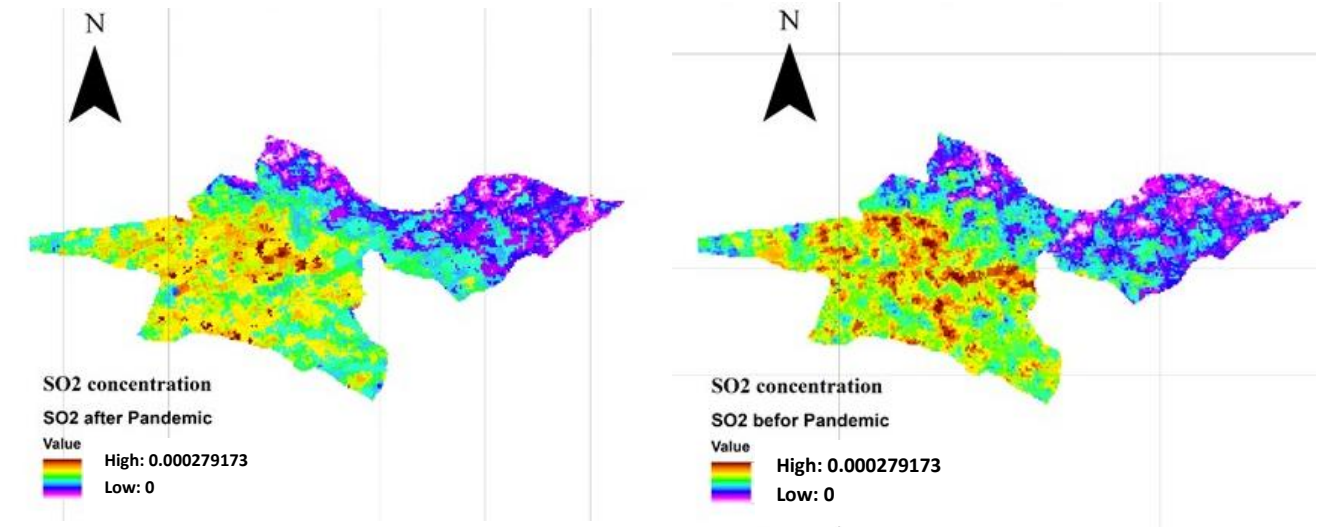

(b)

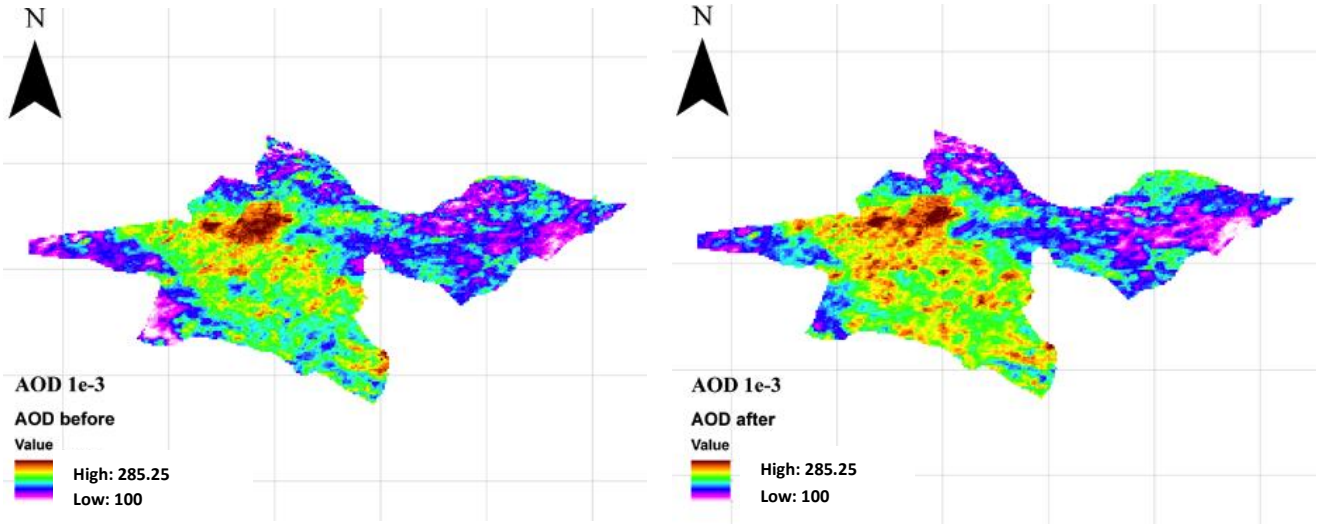

(c)

Fig.3: (a) NOx ,(b) Sox, and (c) AOD yearly median distribution map in Tehran

Figure 3 describes the distribution maps for AOD for these two considered periods. These distribution maps illustrate that Guilan, Khorasan-Razavi, and Tabriz have become more polluted since the pandemic, which is in direct association with the results obtained from Figure 2. Guilan and Khorasan-Razavi are the most tourist regions in Iran due to being adjacent to the Khazar sea and green/ moderate climate for Guilan, and centered on the vast Holy Shrine of Imam Reza (religious pilgrimage) for Khorasan-Razavi.

According to the Figure 2 and Figure 4a&b. Guilan's pollutants trend before and during the pandemic has shown an apparent shift in NO2, SO2, and particle concentration values compared to other cities. Based on the on-site measurement, NO_2, SO_2, and refined PM concentrations in Guilan province varied from 22.38 ppb, 6.98 ppb, and 9.56 µg/m^3 in baseline period the COVID pandemic to 24.81 ppb, 7.30 ppb, and 9.56 14.86 µg/m3 in during COVID pandemic (and before wide and public COVID-19 vaccine), respectively. Moreover, this result is consistent with the previous study that a significant increase of 2.7% was found in the mortality rate due to COVID-19 due to an increase of 1 µg/m^3 of NO_2 [45]. Besides, in Figure 4a. it is shown that the upper line and lower limit of air pollution are not considerable for provinces smaller than Tehran. In contrast, the maximum and minimum of Tehran province are significant in comparison to others. The NO2 concentration has not changed dramatically but climbs in all provinces. This issue shows that COVID Quarantines could not reduce NO_2 concentration. On the other hand, in Figure 4b. the SO_2 concentration in most provinces has increased in maximum concentration, but the minimum and median concentrations did not change in these provinces. With this evidence, it can be concluded that the SO2 condition has become worse than before.

Table 1: SO2, NO2, and AOD column concentrations' means and variances before and during the pandemic

Provinces	correlation factor	Mean 1†	Mean 2‡	Variances 1	Variance 2	ratio of mean values (2/1)	ratio of variance values (2/1)	Air parameters
Isfahan	0.4370	0.0001	0.0001	0.0000	0.0000	1.0402	1.0802	
Tabriz	0.2650	0.0001	0.0001	0.0000	0.0000	1.1509	1.2493	
Khorasan-Razavi	0.5840	0.0001	0.0001	0.0000	0.0000	1.1439	1.0263	SO_2
Tehran	0.6466	0.0001	0.0001	0.0000	0.0000	1.0349	0.8580	
Khuzestan	0.7424	0.0002	0.0002	0.0000	0.0000	0.9526	0.9384	
Guilan	0.3122	0.0001	0.0001	0.0000	0.0000	1.0651	1.3627	
Isfahan	0.9867	0.0001	0.0001	0.0000	0.0000	0.9831	1.2666	
Tabriz	0.9874	0.0001	0.0001	0.0000	0.0000	0.9471	1.0101	
Khorasan-Razavi	0.9921	0.0001	0.0001	0.0000	0.0000	0.9701	1.2382	NO_2
Tehran	0.9923	0.0002	0.0002	0.0000	0.0000	1.0184	1.0901	
Khuzestan	0.9820	0.0001	0.0001	0.0000	0.0000	0.9789	0.9034	
Guilan	0.9881	0.0001	0.0001	0.0000	0.0000	0.9858	1.4046	
Isfahan	0.8028	0.1768	0.1897	0.0208	0.0217	1.0729	1.0415	
Tabriz	0.6267	0.1726	0.1681	0.0006	0.0005	0.9738	0.8661	
Khorasan-Razavi	0.3689	0.1552	0.1653	0.0058	0.0006	1.0654	0.1040	AOD
Tehran	0.8397	0.1834	0.1933	0.0006	0.0008	1.0538	1.3507	
Khuzestan	0.7480	0.2122	0.2279	0.0029	0.0027	1.0739	0.9379	
Guilan	0.2198	0.1955	0.1995	0.0011	0.0013	1.0205	1.1512	

† 1 refers to before pandemic

‡ 2 refers to after pandemic outbreak

3.2. Investigation of pollutants distribution in the base-line period and after the pandemic

The means and variances of air quality parameters in the considered provinces have been presented in Table 1 in study periods. This table shows that Guilan's mean and variance before and during the pandemic have altered considerably. Moreover, in the previous section, we have seen the different trends in satellite components in Guilan province. The monthly median of NO_2 and SO_2 column concentration for Guilan province in two periods was compared. This figure indicates that NO2 concentration in Guilan after the pandemic rose in all months, which seems to be the effect of more travel to this province during the pandemic due to the NO2 sources. However, in the case of Guilan's SO2 concentration, during the second half of the year, SO2 has varied considerably. The monthly RMSE of NOx, SOx, and AOD has been calculated, and their value was 2.5*10-5, $1.4*10^{-4}$, and $1.8*10^{-4}$, respectively.

Table 2: The monthly and seasonal levels of the main signal of $PM_{2.5}$ extracted by wavelet transform in study periods ($\mu g/m^3$)

	Tabriz		**Isfahan**		**Khuzestan**		**Tehran**		**Khorasan Razavi**	
	1†	2‡	1	2	1	2	1	2	1	2
October	19.68	19.87	26.97	31.68	37.14	35.91	25.81	26.49	36.24	27.75
November	15.41	15.81	21.07	28.08	27.64	40.78	21.40	20.73	25.15	24.05
December	11.02	14.13	23.95	21.52	21.41	27.25	13.33	17.95	23.77	17.10
January	10.68	14.08	27.13	24.17	35.26	75.62	17.85	22.81	21.35	16.98
February	10.89	13.11	29.82	23.82	40.84	62.59	23.69	26.63	25.31	19.76
March	15.77	13.03	34.06	31.56	36.00	35.99	32.59	29.61	24.92	28.26
April	13.47	13.25	27.46	31.23	31.31	41.62	27.42	25.43	37.45	25.86
May	10.98	15.94	27.55	26.49	37.78	47.19	24.81	24.68	33.51	25.84
June	18.20	17.85	33.07	31.76	44.92	45.86	30.02	29.44	63.51	35.75
July	18.30	22.70	29.39	40.47	48.21	60.34	32.04	31.22	55.89	42.30
August	19.46	26.50	38.49	49.18	42.47	37.56	38.53	38.78	49.13	38.74
September	23.15	32.93	32.16	57.99	42.10	52.16	33.38	57.71	40.96	44.83
Spring	15.30	16.50	24.06	27.07	28.63	34.69	20.16	21.76	28.41	22.86
Summer	12.46	13.39	30.43	26.62	37.46	57.95	24.64	26.26	23.87	21.56
Fall	14.21	15.65	29.41	29.87	38.10	44.98	27.42	26.56	44.61	29.15
Winter	20.36	27.57	33.40	49.61	44.35	50.15	34.75	42.72	48.86	42.13

† 1 refers to before pandemic

‡ 2 refers to after pandemic outbreak

3.3. Signal decomposition

The wavelet transform was applied to the on-site measurement data sets of $PM_{2.5}$ concentration before and during the COVID-19 pandemic. Figure 4 describes the main signals (a2) of the time series for 5 considered provinces. Moreover, the monthly and seasonal values of the main signals are presented in Table 2 and the standard deviation values of this data (noise) are available in Appendix, A2. The results show that there is a different pattern for two main signals, attributed to two continuous time periods. In the main signal, the PM2.5 concentration almost had higher levels during the COVID-19 outbreak in Tabriz and Khuzestan, by month-to-month comparison. Whereas, PM concentration in Khorasan Razavi has decreased dramatically in all seasons, during the lots of lockdowns in the middle of 2020, compared to the same period in Feb 2019 to Feb 2020 because of a reduction in transport and economic activity. This issue was more visible for seasonal concentration variation of PM in this province. The PM levels were decreased during the COVID pandemic in all months of 2021 except March and September due to lots of Iranian trips to this area during the holidays before the start of the academic year in September and during the Persian New Year holidays in March.

In Isfehan and Tehran, there is no distinct trend by month-to-month comparison. However, the concentration of particulate matter in the metropolitan areas of Iran is higher during the cold seasons of the year due to traffic, fossil fuel sources, and weather conditions [32]. Fine PM has been increased from February 2020 to February 2021, since there were early lockdowns in February 2020 and the restrictions were gradually loosened after July 2020 and starting wide and public COVID-19 vaccine

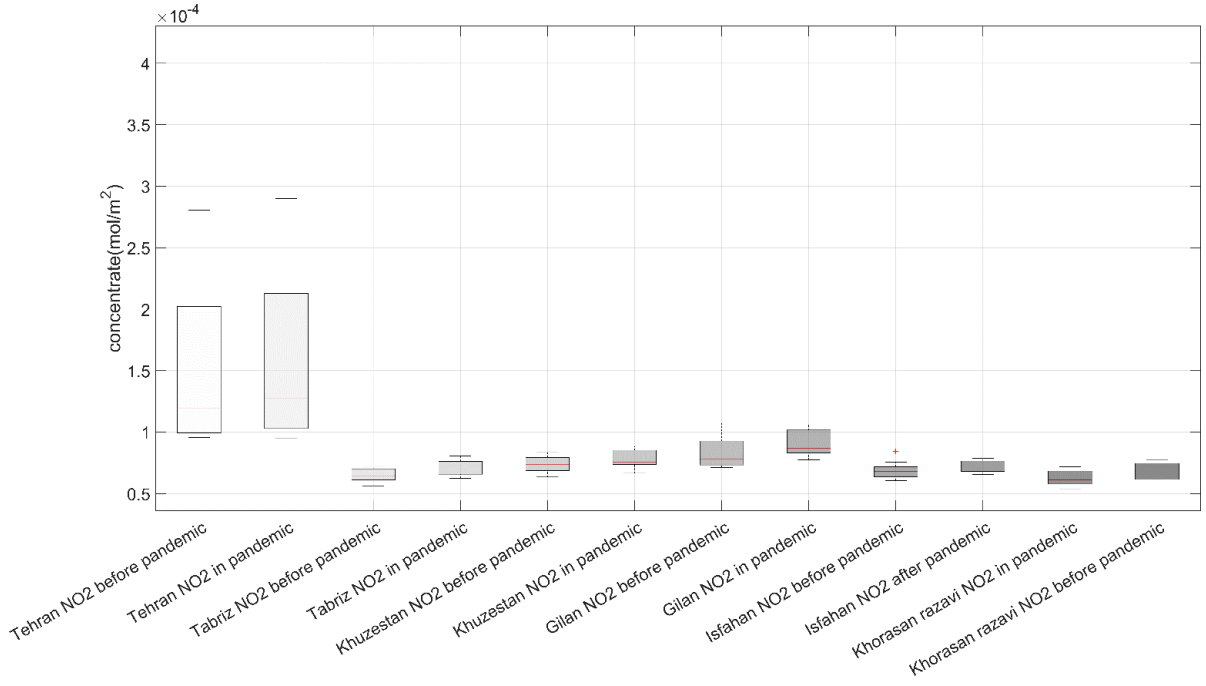

(a)

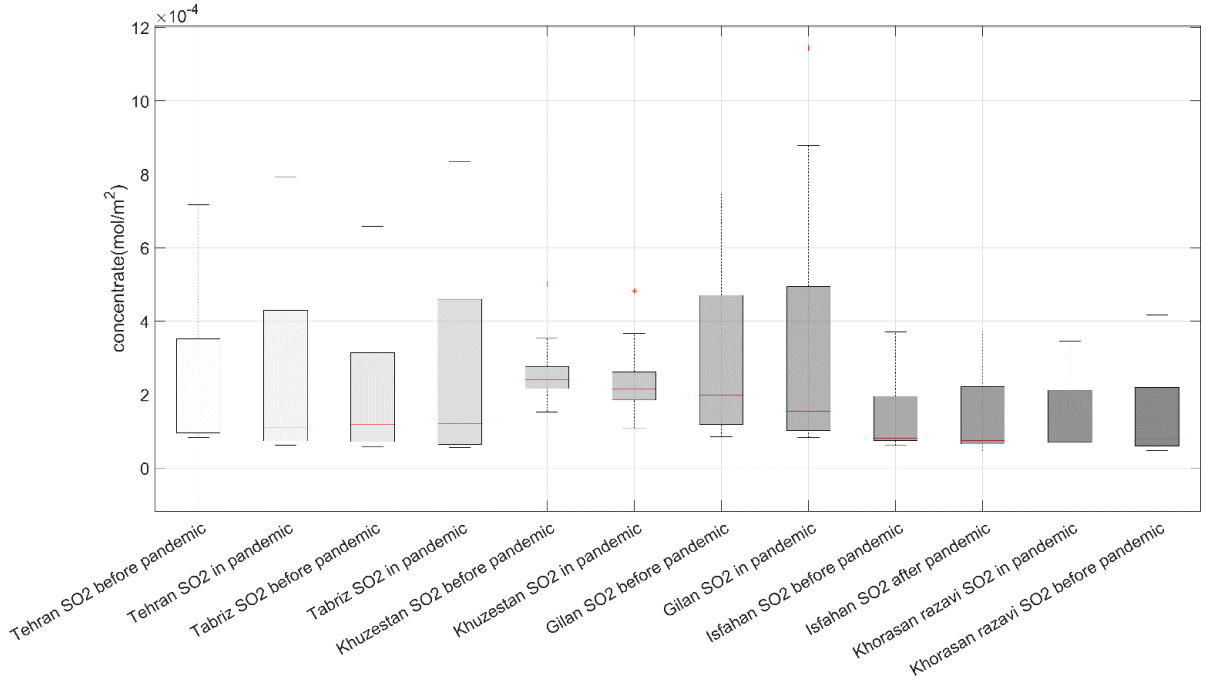

(b)

Fig.4: a) NO_2, b) SO_2 values ranges before and during pandemic

4. Conclusions

The coronavirus disease (COVID-19) pandemic has affected more than 513 million people worldwide. Many studies have shown that air pollutants were significantly reduced with the spread of this pandemic and decreased human and industrial activities due to quarantines or lockdowns. In the present study, the column concentration of NO_2 and SO_2 (two available anthropogenic pollutants) and aerosol optical depth (AOD-represented the extinction of all particles) were examined by using satellite missions (Sentinel-5P and MODIS satellite) in two separate durations (before and during the COVID-19 pandemic) in six central provinces including Isfahan, Tabriz, Mashhad, Tehran, Ahvaz and Guilan in Iran. We utilized the GEE platform to efficiently analyze and visualize large volumes of data

derived from Sentinel and MODIS satellites, providing valuable insights into environmental trends and changes. Regarding the study on spatial and temporal pollutant variation, the ratios of before to during the COVID-19 pandemic for medians of monthly median and variance of NO2, SO2, and AOD values were extracted for two entire years from the 22nd of February 2019 to the 22nd of February, 2021.

The results indicate that the mean ratio of NO_2 remained relatively consistent across the considered provinces over the two-year period, with column concentration ratios ranging from +2% in Tehran to -6% in Tabriz. In contrast, the variance ratio between the two durations showed a more significant change, particularly in Gilan province, a popular tourist destination, even amidst travel restrictions and lockdowns in Iran. In Gilan, NO_2 and SO_2 concentrations increased during the pandemic, driven by heightened travel to the region. Additionally, the AOD distribution map and its trends revealed that Gilan, Khorasan-Razavi, and Tabriz experienced elevated pollution levels following the outbreak, likely due to shifts in tourism patterns and changes in emission sources. These findings offer valuable insights into air pollution dynamics during the COVID-19 pandemic in Iran, providing a deeper understanding of social behaviors and the impact of dominant pollution sources in these areas.

References

[1] Zielinska, B., et al., Emission Rates and Comparative Chemical Composition from Selected In-Use Diesel and Gasoline-Fueled Vehicles. Journal of the Air & Waste Management Association, 2004. 54(9): p. 1138-1150.

[2] Place, S.E. and F.M. Mitloehner, Invited review: Contemporary environmental issues: A review of the dairy industry's role in climate change and air quality and the potential of mitigation through improved production efficiency. Journal of Dairy Science, 2010. 93(8): p. 3407-3416.

[3] Pope, C.A., M. Ezzati, and D.W. Dockery, Fine-Particulate Air Pollution and Life Expectancy in the United States. New England Journal of Medicine, 2009. 360(4): p. 376-386.

[4] Manisalidis, I., E. Stavropoulou, A. Stavropoulos, and E. Bezirtzoglou, Environmental and Health Impacts of Air Pollution: A Review. Frontiers in Public Health, 2020. 8.

[5] Park, J., et al., Reactive oxygen species (ROS) activity of ambient fine particles (PM2.5) measured in Seoul, Korea. Environ Int, 2018. 117: p. 276-283.

[6] Pope, C.A., 3rd, et al., Lung cancer, cardiopulmonary mortality, and long-term exposure to fine particulate air pollution. Jama, 2002. 287(9): p. 1132-41.

[7] Ghorani-Azam, A., B. Riahi-Zanjani, and M. Balali-Mood, Effects of air pollution on human health and practical measures for prevention in Iran. Journal of research in medical sciences : the official journal of Isfahan University of Medical Sciences, 2016. 21: p. 65-65.

[8] Kampa, M. and E. Castanas, Human health effects of air pollution. Environ Pollut, 2008. 151(2): p. 362-7.

[9] Kamali, N., M. Zare Shahne, and M. Arhami, Implementing Spectral Decomposition of Time Series Data in Artificial Neural Networks to Predict Air Pollutant Concentrations. Environmental Engineering Science, 2015. 32: p. 379-388.

[10] Heger, M. and M. Sarraf. Air Pollution in Tehran: Health Costs, Sources, and Policies. 2018.

[11] Yang, J. and B. Zhang, Air pollution and healthcare expenditure: Implication for the benefit of air pollution control in China. Environment International, 2018. 120: p. 443-455.

[12] Liu, Y., et al., Estimating Ground-Level PM2.5 in the Eastern United States Using Satellite Remote Sensing. Environmental Science & Technology, 2005. 39(9): p. 3269-3278.

[13] Goetz, S.J., S.D. Prince, and J. Small, Advances in satellite remote sensing of environmental variables for epidemiological applications, in Advances in Parasitology. 2000, Academic Press. p. 289-307.

[14] NASA, https://daac.ornl.gov/cgi-bin/dsviewer.pl?ds_id=1379. 2022.

[15] EuropeanSpaceAgency, https://sentinels.copernicus.eu/web/sentinel/data-products/-/asset_publisher/fp37fc19FN8F/content/sentinel-5-precursor-level-2-nitrogen-dioxide. 2022.

[16] Briz-Redón, Á. and Á. Serrano-Aroca, The effect of climate on the spread of the COVID-19 pandemic: A review of findings, and statistical and modelling techniques. Progress in Physical Geography: Earth and Environment, 2020. 44(5): p. 591-604.

[17] Bashir, M.F., et al., Correlation between climate indicators and COVID-19 pandemic in New York, USA. Sci Total Environ, 2020. 728: p. 138835.

[18] worldometers. 2022 https://www.worldometers.info/coronavirus/country/iran/].

[19] Faridi, S., et al., A field indoor air measurement of SARS-CoV-2 in the patient rooms of the largest hospital in Iran. Sci Total Environ, 2020. 725: p. 138401.

[20] Wang, S., et al. The Effects of COVID-19 Lockdown on Air Pollutant Concentrations across China: A Google Earth Engine-Based Analysis. International Journal of Environmental Research and Public Health, 2022. 19, DOI: 10.3390/ijerph192417056.

[21] Metya, A., et al., COVID-19 Lockdowns Improve Air Quality in the South-East Asian Regions, as Seen by the Remote Sensing Satellites. Aerosol and Air Quality Research, 2020. 20(8): p. 1772-1782.

[22] Ghasempour, F., A. Sekertekin, and S.H. Kutoglu, Google Earth Engine based spatio-temporal analysis of air pollutants before and during the first wave COVID-19 outbreak over Turkey via remote sensing. Journal of Cleaner Production, 2021. 319: p. 128599.

[23] Ogen, Y., Assessing nitrogen dioxide (NO(2)) levels as a contributing factor to coronavirus (COVID-19) fatality. Sci Total Environ, 2020. 726: p. 138605.

[24] Mesas-Carrascosa, F.-J., et al., Effect of Lockdown Measures on Atmospheric Nitrogen Dioxide during SARS-CoV-2 in Spain. Remote Sensing, 2020. 12(14): p. 2210.

[25] Bigdeli, M., M. Taheri, and A. Mohammadian, Spatial sensitivity analysis of COVID-19 infections concerning the satellite-based four air pollutants levels. Int J Environ Sci Technol (Tehran), 2021. 18(3): p. 751-760.

[26] Hadei, M., et al., Effect of short-term exposure to air pollution on COVID-19 mortality and morbidity in Iranian cities. J Environ Health Sci Eng, 2021. 19(2): p. 1807-1816.

[27] Bagherinia, M., et al., Spatio-temporal air quality assessment in Tehran, Iran, during the COVID-19 lockdown periods. 2023. 38.

[28] Mejía C, D., et al., Spatio-temporal evaluation of air pollution using ground-based and satellite data during COVID-19 in Ecuador. Heliyon, 2024. 10(7): p. e28152.

[29] Saleem, F., et al., Impacts of irregular and strategic lockdown on air quality over Indo-Pak Subcontinent: Pre-to-post COVID-19 analysis. Chaos, Solitons & Fractals, 2024. 178: p. 114255.

[30] Arhami, M., et al., Seasonal trends in the composition and sources of PM2.5 and carbonaceous aerosol in Tehran, Iran. Environmental Pollution, 2018. 239: p. 69-81.

[31] Arhami, M., et al., Seasonal trends, chemical speciation and source apportionment of fine PM in Tehran. Atmospheric Environment, 2017. 153: p. 70-82.

[32] Shahne, M.Z., M. Arhami, V. Hosseini, and I. El Haddad, Particulate emissions of real-world light-duty gasoline vehicle fleet in Iran. Environmental Pollution, 2022. 292: p. 118303.

[33] Zheng, Z., Z. Yang, Z. Wu, and F. Marinello, Spatial Variation of NO2 and Its Impact Factors in China: An Application of Sentinel-5P Products. Remote Sensing, 2019. 11: p. 1939.

[34] Savenets, M., Air pollution in Ukraine: a view from the Sentinel-5P satellite. Idojaras (Budapest, 1905), 2021. 125: p. 271-290.

[35] Kaplan, G. and Z. Yigit Avdan, Space-Borne Air Pollution Observation from Sentinel-5p TROPOMI: Relationship Between Pollutants, Geographical and Demographic Data. 2020.

[36] Hutchison, K.D., S. Smith, and S. Faruqui, The use of MODIS data and aerosol products for air quality prediction. Atmospheric Environment, 2004. 38(30): p. 5057-5070.

[37] Koch, A.C. and L. Bydekerke, Sentinel 5p in the framework of the EU Copernicus programme. 2018. p. 6557.

[38] Ghotbi, S., S. Sotoudeheian, and M. Arhami, Estimating urban ground-level PM10 using MODIS 3km AOD product and meteorological parameters from WRF model. Atmospheric Environment, 2016. 141: p. 333-346.

[39] Xiong, X., et al., NASA EOS Terra and Aqua MODIS on-orbit performance. Advances in Space Research, 2009. 43: p. 413-422.

[40] Musselwhite Thompson, D. and B. Wesolowski, Variance. 2018.

[41] Chai, T. and R.R. Draxler, Root mean square error (RMSE) or mean absolute error (MAE)? – Arguments against avoiding RMSE in the literature. Geosci. Model Dev., 2014. 7(3): p. 1247-1250.

[42] Liu, B., X. Yu, J. Chen, and Q. Wang, Air pollution concentration forecasting based on wavelet transform and combined weighting forecasting model. Atmospheric Pollution Research, 2021. 12(8): p. 101144.

[43] Su, Y., et al., Comparison of air pollution in Shanghai and Lanzhou based on wavelet transform. Environmental Science and Pollution Research, 2019. 26(17): p. 16825-16834.

[44] Akansu, A.N. and R.A. Haddad, Chapter 6 - Wavelet Transform, in Multiresolution Signal Decomposition (Second Edition), A.N. Akansu and R.A. Haddad, Editors. 2001, Academic Press: San Diego. p. 391-442.

[45] Norouzi, N. and Z. Asadi, Air pollution impact on the Covid-19 mortality in Iran considering the comorbidity (obesity, diabetes, and hypertension) correlations. Environmental Research, 2022. 204: p. 112020.

Appendices

A1. Demographic information on the selected area

Province	**Tehran**	**Khuzestan**	**Isfahan**	**Khorasan-Razavi**	**East Azerbaijan**	**Gilan**
Capital City	Tehran	Ahvaz	Isfahan	Mashhad	Tabriz	Rasht
Population (million)	13.3	4.7	5.1	6.4	4	2.5
Mean AOI (during the study period)	100-150	150-200, sometimes over 300	100-150	00-150	80-120	50-100

A2. The monthly and seasonal values of standard deviation (noise) of PM2.5 levels, extracted by wavelet transform in study periods (µg/m3)

	Tabriz		**Isfahan**		**Khuzestan**		**Tehran**		**Khorasan Razavi**	
	1*	2**	1	2	1	2	1	2	1	2
October	6.02	8.26	8.95	10.95	15.85	10.51	9.62	7.86	13.46	8.35
November	3.18	7.63	6.16	7.05	7.83	13.02	4.09	5.60	7.35	4.74
December	2.96	4.72	6.85	4.13	4.91	8.18	3.38	3.27	6.31	7.14
January	1.94	3.77	6.00	2.47	10.90	22.02	4.87	5.63	5.57	4.11
February	2.42	3.37	14.25	3.69	9.32	31.18	4.95	3.81	6.45	5.54
March	2.26	1.87	4.95	9.35	3.59	7.23	5.04	4.32	2.73	7.09
April	2.64	4.77	4.63	4.63	6.61	17.18	4.06	3.63	15.54	5.80
May	3.69	4.26	2.74	3.98	18.02	12.19	2.31	3.85	19.74	4.14
June	2.65	4.75	11.16	5.11	8.72	11.24	4.38	8.91	22.02	8.08
July	6.28	6.40	6.38	11.12	28.15	22.20	7.68	5.74	8.87	13.03
August	6.57	9.10	10.18	15.05	7.20	9.51	12.03	10.54	10.93	13.11
September	5.85	14.30	6.46	14.83	14.30	11.72	10.44	18.86	9.85	11.14
Spring	5.51	7.10	7.75	8.83	12.31	12.03	8.17	6.79	11.01	8.13
Summer	3.24	3.15	9.75	6.95	8.87	27.49	7.88	5.41	5.43	7.29
Fall	4.25	4.98	7.61	5.18	13.40	13.91	4.28	6.34	23.13	7.82
Winter	6.44	11.22	8.76	15.35	18.83	18.19	10.55	17.10	11.61	12.64